

# Lithium in the active sub-giant HD123351

## A quantitative analysis with 3D and 1D model atmospheres using different observed spectra

A. Mott<sup>1</sup>, M. Steffen<sup>1</sup>, E. Caffau<sup>2</sup>, and K. G. Strassmeier<sup>1</sup>

<sup>1</sup> Leibniz-Institut für Astrophysik Potsdam, An der Sternwarte 16, 14482 Potsdam, Germany  
e-mail: amott@aip.de

<sup>2</sup> GEPI, Observatoire de Paris, PSL Research University, CNRS, Place Jules Janssen, 92195, Meudon France.

**Abstract.** Current 3D hydrodynamical model atmosphere simulations together with non-LTE spectrum synthesis calculations permit to determine reliable atomic and in particular isotopic chemical abundances. Although this approach is computationally time demanding, it became feasible in studying lithium in stellar spectra. In the literature not much is known about the presence of the more fragile <sup>6</sup>Li isotope in evolved metal-rich objects. In this case the analysis is complicated by the lack of a suitable list of atomic and molecular lines in the spectral region of the lithium resonance line at 670.8 nm.

Here we present a spectroscopic comparative analysis of the Li doublet region of HD 123351, an active sub-giant star of solar metallicity. We fit the Li profile in three observed spectra characterized by different qualities: two very-high resolution spectra (Gecko@CFHT,  $R=120\,000$ ,  $\text{SNR}=400$  and PEPSI@LBT,  $R=150\,000$ ,  $\text{SNR}=663$ ) and a high-resolution SOPHIE@OHP spectrum ( $R=40\,000$ ,  $\text{SNR}=300$ ). We adopt a set of model atmospheres, both 3D and 1D, having different stellar parameters ( $T_{\text{eff}}$  and  $\log g$ ). The 3D models are taken from the CIFIST grid of CO5BOLD model atmospheres and departures from LTE are considered for the lithium components. For the blends other than the lithium in this wavelength region we adopt the linelist of Meléndez et al. (2012). We find consistent results for all three observations and an overall good fit with the selected list of atomic and molecular lines, indicating a high <sup>6</sup>Li content. The presence of <sup>6</sup>Li is not expected in cool stellar atmospheres. Its detection is of crucial importance for understanding mixing processes in stars and external lithium production mechanisms, possibly related to stellar activity or planetary accretion of <sup>6</sup>Li-rich material.

**Key words.** Stars: abundances – Stars: atmospheres – Line: profiles – Stars: HD 123351

### 1. Introduction

HD 123351 is an active sub-giant, primary member of a single-lined spectroscopic binary system with high eccentricity ( $e = 0.809$ ) that was firstly analyzed by Strassmeier et al. (2011) who derived the fundamental stel-

lar parameters ( $T_{\text{eff}} = 4800$  K,  $\log g = 3.2$  dex,  $[\text{Fe}/\text{H}] = 0.00$  dex). They found a 1D lithium abundance of  $A(\text{Li}) = (1.70 \pm 0.05)$  dex from a high-resolution Gecko spectrum, allowing for departures from Local Thermodynamic Equilibrium (NLTE). More recently, Mott et

al. (2017) determined both  $A(\text{Li})$  and the  ${}^6\text{Li}/{}^7\text{Li}$  isotopic ratio from the same Gecko spectrum by means of 3D and 1D model atmospheres, different fitting setups, and a sample of lists of atomic and molecular data. They find an amount of lithium in agreement with Strassmeier et al. (2011) and a significant  ${}^6\text{Li}$  content of  $10.6 \pm 4.11\%$  in 3D NLTE. In this work we present a similar spectroscopic analysis of the  $\text{Li I}$  resonance doublet at 670.8 nm in HD 123351, using not only the Gecko spectrum but also a lower resolution SOPHIE spectrum and a preliminary, very-high resolution PEPSI spectrum. Since the data are obtained at different epochs, this can be useful in understanding if there is any variation of the lithium line profile with the orbital phase of the star. Moreover, we adopt 1D and 3D model atmospheres with different temperatures and gravities to test the impact of stellar parameters on the derived atomic and isotopic abundances.

## 2. Observational data

The observed spectra of the lithium resonance doublet at 670.8 nm are acquired with three different instruments representing different qualities in terms of signal-to-noise ratio (SNR) and resolving power ( $R$ ):

- SOPHIE@OHP (Provence, France):  $R=40\,000$ ,  $\text{SNR}=300:1$ , taken in March 2014 (hereafter SOPHIE, Perruchot et al. 2008, 2011);
- Gecko@CFHT (Hawaii, US):  $R=120\,000$ ,  $\text{SNR}=400:1$ , taken in May 2000 (Gecko);
- PEPSI@LBT (Arizona, US):  $R=150\,000$ ,  $\text{SNR}=663:1$ , taken in April 2015 (PEPSI, Strassmeier et al. 2015).

The PEPSI spectrum is the outcome of a preliminary data reduction and it is not yet in its final optimal form. This is due to the fact that the PEPSI instrument is still in the commissioning phase and its pipeline is constantly being improved. In a forthcoming paper we will present an analysis of several fully reduced PEPSI spectra of HD123351.

We point out that each spectrum is the result of an independent data reduction carried

out with distinct pipelines and with their own continuum normalization.

It is well known that the placement of the continuum can affect the evaluation of, above all, rather delicate quantities like the  ${}^6\text{Li}/{}^7\text{Li}$  ratio but also of individual chemical abundances.

This is especially true in high-metallicity cool stars in which the interference of several atomic and molecular lines can impede the correct identification of the continuum level. For this reason the contribution of the continuum placement will be included in the uncertainties on the final results, for both  $A(\text{Li})$  and  ${}^6\text{Li}/{}^7\text{Li}$ . Doing a spectroscopic investigation of the lithium region by using multiple observed data and comparing the final results with each other can give an idea of the impact of the quality of the input observed spectrum on the accuracy of the lithium analysis.

### 2.1. Comparison of the observed data

Fig. 1 shows the observed spectra used in this work, superimposed on the reference solar flux atlas by Kurucz (2005). The two very-high resolution spectra (Gecko and PEPSI) exhibit good agreement with each other, especially in the red wing of the resonance lithium doublet where the  ${}^6\text{Li}$  components lie, despite some small differences that can be noted elsewhere. The line core of the  $\text{Li I}$  line in the PEPSI spectrum seems to be slightly deeper and narrower than in the Gecko spectrum; this is attributed to their different resolving power. Such behavior has been confirmed examining the shape of other strong isolated absorption lines including tellurics. The  $\text{Fe I}$  feature at 670.74 nm, which constitutes the dominant contribution to the blend, appears in PEPSI slightly different than in Gecko, both in shape and in residual intensity. The parallel analysis of the two spectra can be used for probing the impact of such blend feature on both the lithium abundance  $A(\text{Li})$  and  ${}^6\text{Li}/{}^7\text{Li}$  ratio. The SOPHIE overall profile is naturally broader than the other two due to its lower resolving power.

Although we do not expect dramatic differences in the final values for  $A(\text{Li})$  and the  ${}^6\text{Li}/{}^7\text{Li}$  isotopic ratio using the two very-high

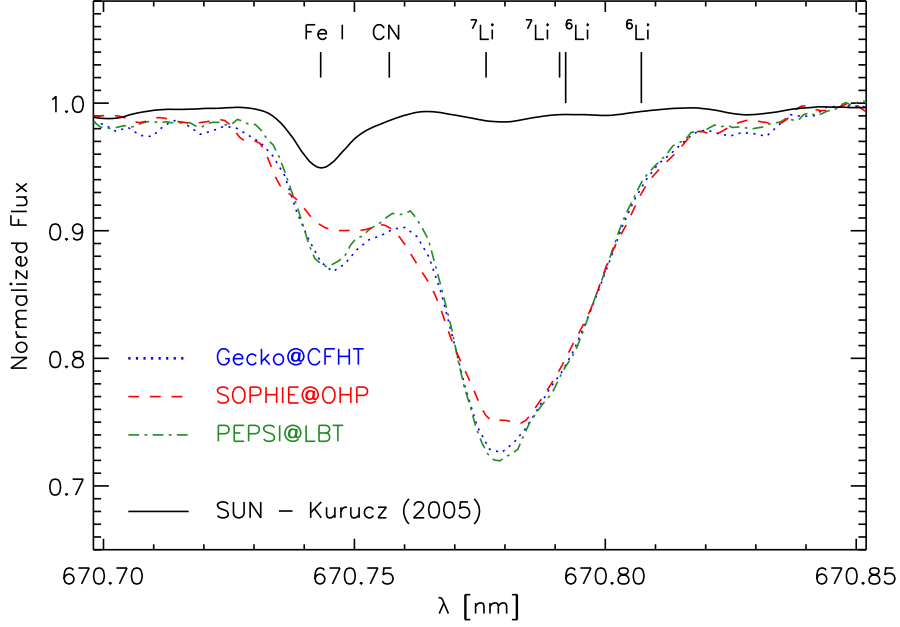


**Fig. 1.** Comparison of observed spectra of the Li doublet region of HD 123351 around 670.8 nm. The Gecko (blue dotted line), SOPHIE (red dashed line) and PEPSI (green dashed-dotted line) spectra are superimposed on the Solar flux atlas by Kurucz (2005) (black continuous line) for a comparison. The locations of the Li I components and the dominant blends attributed to Fe I and CN are also indicated.

resolution spectra due to their fairly good accordance, we emphasize the importance of carrying out the complete lithium isotopic and abundance determination by using different observed data in the fitting procedure, conferring in this way robustness and additional credibility to the final results.

In Fig. 2 we show the STELLA radial velocities phased with the orbital period of HD 123351 ( $P_{\text{orb}} = 149.1819$  d). This figure has been taken from Strassmeier et al. (2011), and the added data points indicate the orbital phase ( $\phi_{\text{obs}}$ ) at which our three observed spectra were taken. The three phases were computed knowing the Julian date  $HJD_{\text{obs}}$  of each observation, the period of the periastron  $T_{\text{per}}$  (defined as the minimum distance between the two stars of the binary system) and the orbital period of the star  $P_{\text{orb}}$  (Strassmeier et al. 2011)

by means of the equation:

$$\phi_{\text{obs}} = \left\{ \frac{HJD_{\text{obs}} - T_{\text{per}}}{P_{\text{orb}}} \right\}, \quad (1)$$

where the curly brackets denote the fractional part of the resulting number. The peak at phase 1.0 corresponds to the moment at which the star reaches the periastron of the orbit. From the diagram we note that all three spectra, although they are representative of different stellar orbital phases, show roughly the same radial velocity of  $V_r \sim -12.00$  km s<sup>-1</sup>. Even in the case of possible orbital modulation, we do not expect large discrepancies in the final derived  $A(\text{Li})$  and  ${}^6\text{Li}/{}^7\text{Li}$  isotopic ratio since none of the spectra is taken close to periastron.

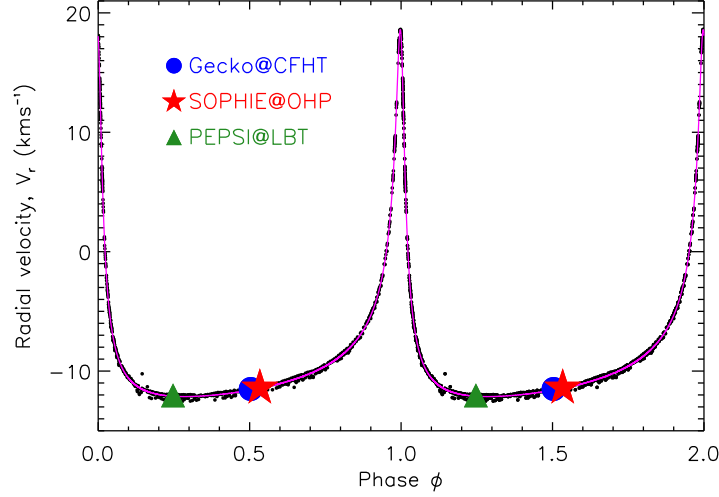


**Fig. 2.** Phased STELLA radial velocities of HD 123351. Black dots are the observations and the orbital Keplerian fit is indicated with the magenta line. The colored symbols represent the orbital phase (for phases  $\phi_{\text{obs}}$  and  $\phi_{\text{obs}} + 1$ ) at which the three observational spectra have been taken (Eq. 1).

**Table 1.** List of 3D C05BOLD models and associated 1DLHD model atmospheres used for HD 123351.

Model name	Label	Type	$T_{\text{eff}}$ [K]	$\log g$ cgs	[Fe/H] dex	Box size X×Y×Z	Geom. size X×Y×Z [Mm]	# Snaps
d3t48g32mm00n01	a	3D	$4777 \pm 10$	3.20	0.00	$200^2 \times 140$	$109.7^2 \times 35.2$	20
t4780g32mm00a05cifist	b	1D LHD	4780	3.20	0.00	–	–	–
d3t46g32mm00n01	c	3D	$4583 \pm 13$	3.20	0.00	$200^2 \times 140$	$109.7^2 \times 35.2$	22
t4580g32mm00a05	d	1D LHD	4580	3.20	0.00	–	–	–
d3gt46g35n03	e	3D	$4552 \pm 10$	3.50	0.00	$200^2 \times 140$	$109.7^2 \times 35.2$	12
t4550g35mm00ml3a05	f	1D LHD	4550	3.50	0.00	–	–	–

### 3. Model atmospheres and line formation

In this work we compute synthetic spectra of the lithium doublet feature at 670.8 nm adopting different model atmospheres. For the 3D models, we use a sub-set of the CIFIST atmosphere grid (Ludwig et al. 2009) computed with the code C05BOLD (Freytag et al. 2012). For the one-dimensional models, we used the 1DLHD models (Caffau & Ludwig 2007) that are associated to each 3D model. This is the preferred choice when it is neces-

sary to perform a comparative spectroscopic analysis since the two type of models differ exclusively in terms of the treatment of the convection and not in the micro-physics and numerics involved (equation of state, opacities, radiative transfer scheme). The models are the same as those used in Mott et al. (2017) and their properties are listed in Table 1. We used the package `Linfor3D`<sup>1</sup> to compute a grid of synthetic lithium line profiles in 3D and 1D

<sup>1</sup> <http://www.aip.de/Members/msteffen/linfor3d>

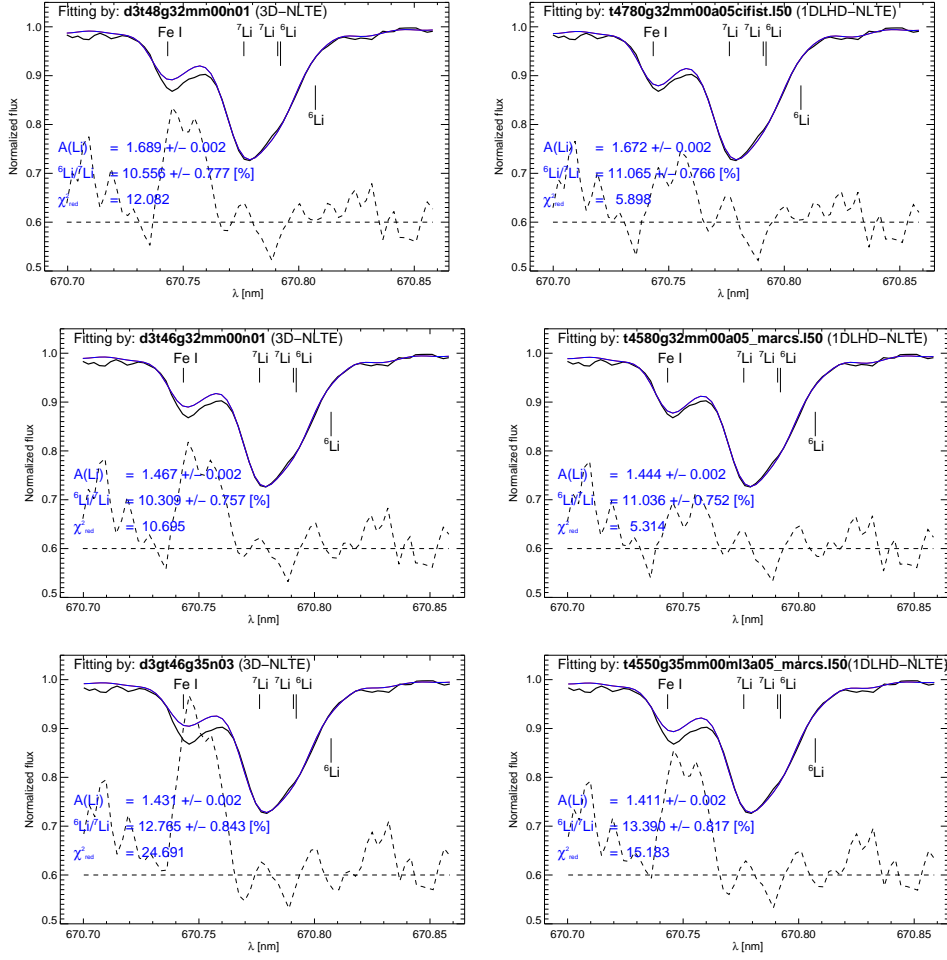


**Fig. 3.** Best-fits (blue line) of the Gecko spectrum (continuous black line) achieved with the models listed in Table 1 and labeled accordingly. The quality of each fit is expressed by means of the  $\chi^2_{\text{red}}$ . The residuals, magnified by a factor 10 for better visualization, are shown as dashed line. The error bars on  $A(\text{Li})$  and  ${}^6\text{Li}/{}^7\text{Li}$  are the formal internal fitting error ( $1\sigma$ ), for the final uncertainties see Table 2.

with a range of  $A(\text{Li})$  and  ${}^6\text{Li}/{}^7\text{Li}$  ratios. We assume NLTE for the Li components and LTE for the blends for which we adopted the linelist of Meléndez et al. (2012). This list of atomic and molecular blend lines has been confirmed by Mott et al. (2017) to be the currently best linelist for reproducing the Li I  $\lambda 670.8$  nm region in this particular star. The fitting procedure is extensively described in the aforemen-

tioned paper. In this work we focused on the Full range only that includes all the blends between 670.70 nm and 670.86 nm in addition to the Li I resonance feature.

#### 4. Results

In this Section we present the best-fits we obtained from the least square fitting minimization analysis (we refer to Mott et al. 2017 for

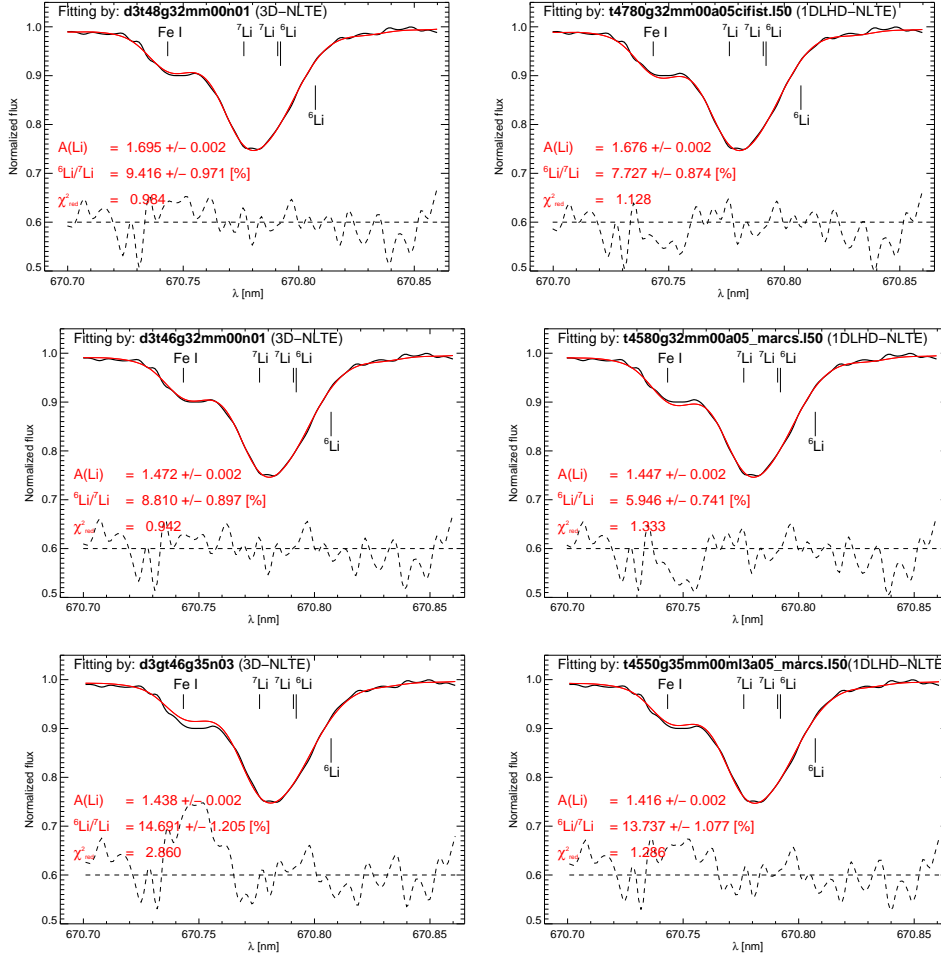


**Fig. 4.** Same as Fig. 3 but for the SOPHIE spectrum. Best-fits are shown as red solid lines.

details about the fitting procedure). We plot in Fig. 3, 4 and 5 the fits to the Gecko (in blue), SOPHIE (in red) and PEPSI (in green) spectra. The six panels show the fits for the model atmosphere listed in Table 1, with the 3D NLTE and 1D NLTE results on the left and right side respectively. We underline that the fitting procedure was kept the same for all fits (set of free parameters, continuum fixed to 1.00 and  $v \sin i$  equal to  $1.8 \text{ km s}^{-1}$  as derived in Strassmeier et al. 2011). The final results, presented in Table 2, refer to the best-fit values for  $A(\text{Li})$  and the

${}^6\text{Li}/{}^7\text{Li}$  isotopic ratio obtained adopting the 3D and 1D LHD model atmospheres with stellar parameters closest to those of the target star ( $T_{\text{eff}}/\log g/[\text{Fe}/\text{H}]=4800/3.2/0.00$ ). In the last four columns of the same Table, it is possible to examine the different sources of errors that were later-on combined to obtain the final error bars on the atomic and isotopic abundances. To evaluate  $\sigma_{T_{\text{eff}}}$ , the systematic uncertainty due to a change in temperature in the input model atmospheres of  $\Delta T_{\text{eff}} = \pm 100 \text{ K}$ , we took the semi-difference between the  $A(\text{Li})$  and  ${}^6\text{Li}/{}^7\text{Li}$

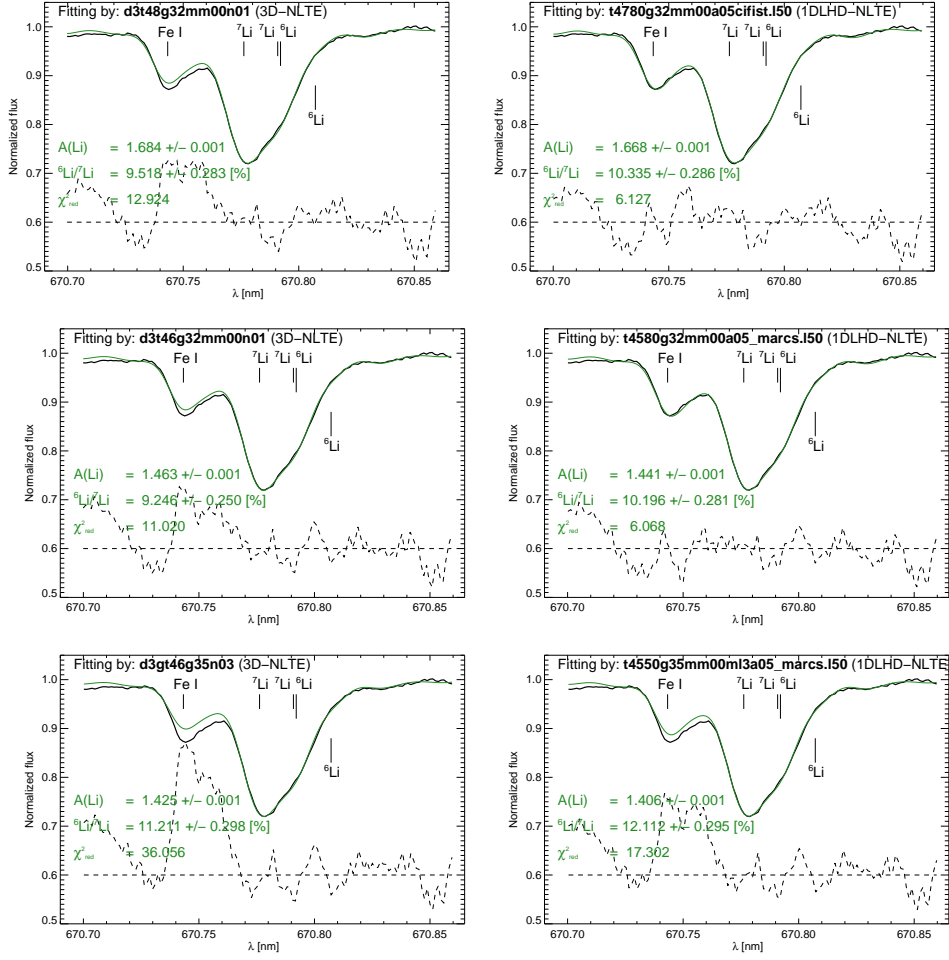


**Fig. 5.** Same as Fig. 3 but for the PEPSI spectrum. Best-fits are shown as green solid lines.

displayed in panels *a* and *c* of Figures 3, 4 and 5, for the 3D case, and panels *b* and *d* for 1D. The assumed  $\Delta T_{\text{eff}}$  is consistent with the 70 K error bars of the spectroscopically derived  $T_{\text{eff}}$  of HD 123351, as listed in Table 3 of Strassmeier et al. (2011). Similarly, we calculated  $\sigma_{\log g}$  from the quantities presented in panels *c* and *e* (for 3D) and panels *d* and *f* (for 1D) of the same Figures with a variation ( $\Delta \log g$ ) of  $\pm 0.15$  dex in surface gravity.

The results for the Gecko spectrum have been previously discussed in Mott

et al. (2017) giving as best fit values, with the linelist of Meléndez et al.

(2012),  $A(\text{Li}) = (1.69 \pm 0.11)$  dex and  ${}^6\text{Li}/{}^7\text{Li} = 10.56 \pm 2.52\%$  in 3D NLTE. For the SOPHIE and PEPSI data, we find compatible values that fall well within the respective errorbars (Table 2). In the 1D NLTE fits, the derived lithium abundances are almost equal to the 3D NLTE values, but a larger spread can be noted in the  ${}^6\text{Li}/{}^7\text{Li}$  value. This is more evident in the SOPHIE spectrum where also the associated error bar appears to be larger

**Table 2.** Best-fit results for the three observed spectra used in this work and the models *a* and *b* of Table 1. The uncertainties indicated in the last four columns are summed up in quadrature to generate the final errorbars on the  $A(\text{Li})$  and  ${}^6\text{Li}/{}^7\text{Li}$  ratio (column three).

Gecko			$\sigma_{T_{\text{eff}}}$	$\sigma_{\log g}$	$\sigma_{\text{fit}}$	$\sigma_{\text{cont.}}$
3D-NLTE (a)	$A(\text{Li})$	$1.69 \pm 0.11$	0.111	0.018	0.002	0.012
	${}^6\text{Li}/{}^7\text{Li}$	$10.56 \pm 2.52$	0.124	1.228	0.777	2.060
1D-NLTE (b)	$A(\text{Li})$	$1.67 \pm 0.11$	0.114	0.017	0.002	0.007
	${}^6\text{Li}/{}^7\text{Li}$	$11.06 \pm 1.94$	0.015	1.177	0.766	1.338
SOPHIE						
3D-NLTE (a)	$A(\text{Li})$	$1.69 \pm 0.11$	0.112	0.017	0.002	0.001
	${}^6\text{Li}/{}^7\text{Li}$	$9.42 \pm 3.11$	0.303	2.941	0.971	0.083
1D-NLTE (b)	$A(\text{Li})$	$1.68 \pm 0.13$	0.115	0.016	0.002	0.004
	${}^6\text{Li}/{}^7\text{Li}$	$7.73 \pm 4.34$	0.891	3.896	0.874	1.454
PEPSI						
3D-NLTE (a)	$A(\text{Li})$	$1.68 \pm 0.11$	0.111	0.019	0.001	0.005
	${}^6\text{Li}/{}^7\text{Li}$	$9.52 \pm 1.30$	0.136	0.983	0.283	0.784
1D-NLTE (b)	$A(\text{Li})$	$1.67 \pm 0.12$	0.114	0.018	0.001	0.001
	${}^6\text{Li}/{}^7\text{Li}$	$10.33 \pm 1.00$	0.070	0.958	0.286	0.065

compared to the results from the very-high resolution spectra. This can be seen as an indication that the use of lower resolution data leads to a more uncertain value of the measured  ${}^6\text{Li}/{}^7\text{Li}$  isotopic ratio, confirming that a reliable isotopic analysis requires the highest possible spectral resolution ( $R \geq 100\,000$ ). Nevertheless, it is worth noting that even our analysis of the SOPHIE spectrum indicates a detection of the  ${}^6\text{Li}$  isotope that is in remarkable agreement with our findings based on the Gecko and PEPSI spectra.

From Figures 3, 4, and 5 we note that by using the cooler 3D model *c*, the lower temperature plays the important role of decreasing the lithium abundance of roughly 0.2 dex for all the observed spectra. This translates into the major contribution to the final uncertainty of the derived  $A(\text{Li})_{3\text{DNLTE}}$ , as can be seen in the fourth column of Table 2. On the other hand, a higher gravity in the input model intervenes mainly in fitting the line profile with a higher  ${}^6\text{Li}/{}^7\text{Li}$  ratio rather than changing the atomic abundance. This can be seen, e.g. for the Gecko spectrum, comparing panels *c* and *e* of Fig. 3

(and analogously in Fig. 4 and 5 for SOPHIE and PEPSI, respectively) for the 3D case, and panels *d* and *f* for the 1D case. Therefore, for the isotopic ratio, the major contribution to the total error bar is imputable to the systematic uncertainty on the  $\log g$  parameter of the input model atmosphere.

## 5. Conclusions

The results in terms of  $A(\text{Li})$  and  ${}^6\text{Li}/{}^7\text{Li}$  ratio determined from the three different spectra are found to be in quite good agreement with each other (well within the respective error bars) although the observed spectra are of different qualities (signal-to-noise ratio and spectral resolution). The lower resolution SOPHIE spectrum leads to larger error bars of the lithium isotopic ratio but it still yields a reasonable estimate of the  ${}^6\text{Li}/{}^7\text{Li}$  ratio. It also provides a robust atomic lithium abundance that is in concordance with Gecko and PEPSI results.

This comparative analysis of three independent observed spectra eliminates the possibility that the detected  ${}^6\text{Li}$  in HD 123351 could



be an artifact related to the particular Gecko spectrum that has been analyzed in Mott et al. (2017). Trusting in the line list of Meléndez et al. (2012), there is no way around the conclusion that the isotopic ratio of HD 123351 is roughly  ${}^6\text{Li}/{}^7\text{Li} \approx 10\%$ . Such high  ${}^6\text{Li}$  content challenges stellar evolution theories since they do not predict the presence of this lithium isotope in an evolved object like our target star, but rather its total destruction. The initial  ${}^6\text{Li}$  present in the interstellar medium is not able to survive at the high temperatures at the base of the convective stellar envelope during the pre-main sequence phase. External mechanisms need to be invoked to explain its presence in the atmosphere of this star. Potential sources of  ${}^6\text{Li}$  may be related to energetic stellar flares or to the existence of a planetary system which somehow enables the fairly recent accretion of Li-rich rocky material onto the star.

The question about the origin of the  ${}^6\text{Li}$  content in evolved cool stars is difficult to answer based on the analysis of a single case. Rather, it is necessary to investigate larger samples of stars to look for correlations between

the  ${}^6\text{Li}$  content and the level of magnetic activity and/or the presence of a planetary system. This sort of analysis can also help to clarify the validity of mixing-related lithium production scenarios in post Main Sequence objects.

## References

- Caffau, E., Ludwig, H.-G. 2007, *A&A*, 467, 11  
 Freytag, B., Steffen, M., Ludwig, H.-G., et al. 2012, *J. Comp. Phys.*, 231, 919  
 Kurucz, R. L. 2005, *MSAIS*, 8, 189  
 Ludwig, H.-G., Caffau, E., Steffen, M., et al. 2009, *MmSAI*, 80, 711  
 Meléndez, J., Bergemann, M., Cohen, J. G., et al. 2012, *A&A*, 543, 29  
 Mott, A., Steffen, M., Caffau, E., et al. 2017, *A&A*, submitted  
 Perruchot, S., Kohler, D., Bouchy, F., et al. 2008, *Proc. SPIE*, 7014, 70140  
 Perruchot, S., Bouchy, F., Chazelas, B., et al. 2011, *Proc. SPIE*, 8151, 815115  
 Strassmeier, K. G., Carroll, T. A., Weber, M., et al. 2011, *A&A*, 535, 98  
 Strassmeier, K. G., Ilyin, I., Järvinen, A., et al. 2015, *Astron. Nachr.*, 336, 324